VFD Machinery Vibration Fatigue Life and Multilevel Inverter Effect

Xu Han and Alan B. Palazzolo

***Abstract*—This paper documents fatigue-related mechanical failures in variable-frequency drive (VFD) motor machinery due to mechanical vibrations excited by drive torque harmonics which are created by pulse width modulation (PWM) switching. Present effort models the coupled system with a full electrical system (including the rectifier, dc bus, inverter, and motor), and an industrial mechanical system (including flexible couplings, gearboxes, and multiple inertias). The models are formed by a novel combination of a commercial motor code with a general self-written mechanical code. The approach extends failure prediction beyond the simple occurrence of resonance to fatigue life evaluation based on the rain-flow algorithm, which is suitable for both steady state and transient start-up mechanical response. The second contribution is a demonstration that the common use of a multilevel inverter to reduce voltage/current harmonics may actually exacerbate resonance and fatigue failure. This is shown to be caused by a resulting amplitude increase of torque components in proximity to potential resonance frequencies.**

***Index Terms*—Fatigue, rain-flow, variable-frequency drive (VFD), vibration.**

I. Introduction

PREVIOUS papers in this area ascertained failure based only on whether coincidence (resonance) of a variable-frequency drive (VFD) torque harmonic frequency and a mechanical natural frequency occurred and provided examples with models of relatively simple machinery trains. The shortcomings of this approach are that damping may act to mitigate fatigue failure even with resonance, the amplitude of the torque harmonic at resonance may be too small to cause large stresses, high stresses due to resonance may occur only for a brief period during the start-up of the motor, and the approach does not provide the time or number of cycles (events) to failure. Machinery trains possess torsional vibration damping that originates in specialized couplings that connect the machinery components and/or have torque harmonics that are insignificant. Thus, judging that a machine will fail based solely on the coincidence of a torque harmonic and a natural frequency may overly constrain the design. A better design practice is to predict damage and life based on the simulated torsional stress response to VFD motor-induced mean and alternating stresses.

Manuscript received November 12, 2012; accepted February 26, 2013. Date of publication June 3, 2013; date of current version November 18, 2013. Paper 2012-EMC-620, presented at the 2012 IEEE Industry Applications Society Annual Meeting, Las Vegas, NV, USA, October 7–11, and approved for publication in the IEEE Transactions on Industry Applications by the Electric Machines Committee of the IEEE Industry Applications Society.

The authors are with the Department of Mechanical Engineering, Texas A&M University, College Station, TX 77840 USA (e-mail: hanxu_zju@tamu.edu; a-palazzolo@tamu.edu).

Digital Object Identifier 10.1109/TIA.2013.2265871

II. Literature Review

The literature on vibration control and life prediction in non-VFD torsional vibration machinery trains is quite extensive. For instance, the transitory torsional resonance of a conventional drive synchronous motor machinery train due to a dynamic torque at twice the slip frequency is discussed in [1]–[3]. VFD-related torque harmonics and their causes have been analyzed in several references [4], [5]. Holmes [4] provides theoretical expressions for the torque harmonic frequencies as a function of the pulse width modulation (PWM) switching frequency. Inverter control-induced torque harmonics, including the first, second, and sixth torque harmonics, are analyzed in [5]. This reference also considers the dc component of phase current, asymmetric deadtime voltage, and magnetic saturation, which play important roles in generating torque harmonics.

Torsional machinery vibration problems related to the usage of VFDs were reported as early as the 1980s [6]. The case history in [7] verified the earlier predictions with actual test field operation measurements. This was followed by a series of papers documenting failures that occurred in industrial VFD machinery trains [8]–[13]. The measurements in [7] showed that the incorporation of the VFD resulted in a significant increase in torsional vibration. Accurate prediction of the VFD-related torque harmonics at the design stage was a formidable task, in part due to their dependence on the power switch type, control law, measurement sensor, electrical and mechanical system interactions, etc. This caused a high uncertainty in reliability prior to the actual operation of the machinery.

Some VFD-related research shows that the reduction of the total harmonic distortion (THD) is possible by implementing higher level inverter schemes [14], [15]. Although this is true and also beneficial from the standpoint of reducing electromagnetic interference (EMI) and ohmic losses, it does not guarantee that all components of torque are reduced, and as shown by our example, certain harmonics may actually increase as the inverter level increases and further exacerbate a high-cycle fatigue problem. A recent publication [16] provides formulas for the torque harmonic frequencies and the relationships between torque and current harmonic frequencies, which are verified by both simulations and tests. These authors develop a particularly clever approach for eliminating entire series of torque harmonics by implementing a PWM carrier frequency interleaving on a four-thread VFD. A possible drawback to this approach is an

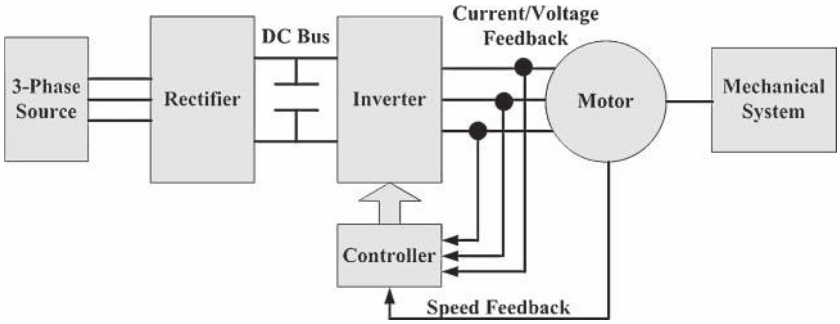

Fig. 1. VFD machinery train with VSI.

increase in hardware cost and lower reliability. The example presented here demonstrates alternative approaches for mitigating the effects of a problematic torque harmonic by increasing the damping in the machinery couplings or by changing the PWM switching frequency or the electrical frequency.

Although the aforementioned references provide excellent treatment for the determination of VFD-related dynamic torques, they lack a means for predicting vibrations and life of a complete machinery train that has significant coupling between its mechanical and electrical subsystems. This task is addressed by the present approach that includes a high fidelity total system model and analysis that extends from the three-phase power input source of the dc bus to the torsional stresses and fatigue life of all mechanical components. This enables one to optimize the design of a torsional machinery system by selecting parameter values from a parameter space which includes mechanical parameters (such as moments of inertias, coupling stiffness, etc.), and electrical parameters (such as IGBTs, motor stator inductances and resistances, etc.), in order to extend life. The prediction of life is based on a rain-flow stress cycle counting process that is applicable to transient phenomena such as start-ups or steady-state harmonic near-resonance vibration.

III. Theory

A. VFD System

A complete VFD machinery system can be divided into two major subsystems—electrical and mechanical—as shown in Fig. 1.

The electrical–mechanical subsystem interface is the electrical motor. The electromagnetic torque is generated inside the motor due to electromagnetic interactions, and the motor rotor is part of the mechanical system. The mathematical model of an induction motor shown hereinafter employs the q-d frame [17] approach, which is obtained by coordinate transformation from a three-phase a-b-c frame.

Kirchoff's voltage balance equations are as follows:

$$v_{ds} = r_s i_{ds} + d/dt\lambda_{ds} - \omega\lambda_{qs} \tag{1}$$

$$v_{qs} = r_s i_{qs} + d/dt\lambda_{qs} + \omega\lambda_{ds} \tag{2}$$

$$v'_{dr} = r'_r i'_{dr} + d/dt\lambda'_{dr} - (\omega - \omega_r)\lambda'_{qr} \tag{3}$$

$$v'_{qr} = r'_r i'_{qr} + d/dt\lambda'_{qr} + (\omega - \omega_r)\lambda'_{dr}. \tag{4}$$

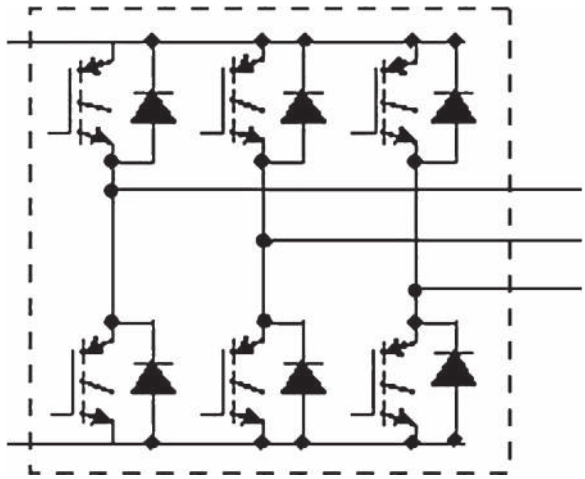

Fig. 2. Two-level inverter topology.

Flux-current relation equations are as follows:

$$\lambda_{ds} = L_{ls} i_{ds} + L_m \left(i_{ds} + i'_{dr}\right) \tag{5}$$

$$\lambda_{qs} = L_{ls} i_{qs} + L_m \left(i_{qs} + i'_{qr}\right) \tag{6}$$

$$\lambda'_{dr} = L'_{lr} i'_{dr} + L_m \left(i_{ds} + i'_{dr}\right) \tag{7}$$

$$\lambda'_{qr} = L'_{lr} i'_{qr} + L_m \left(i_{qs} + i'_{qr}\right). \tag{8}$$

Torque-current relation equations are as follows:

$$T_e = \frac{3}{2}\frac{P}{2} L_m \left(i_{qs} i'_{dr} - i_{ds} i'_{qr}\right) \tag{9}$$

where v and i represent voltage and current qualities, respectively; r, L, and λ represent resistance, inductance, and flux qualities, respectively; subscripts q and d indicate q- and d-axis components, respectively; subscripts s and r indicate stator and rotor components, respectively; subscript m indicates the magnetizing component; superscript $'$ indicates the turn ratio transformation; ω_r is the rotor angular velocity in radians per second; T_e is the electromagnetic torque; and P is the number of pole pairs.

The three-phase ac voltage source provides electric power to the entire system. This voltage is applied to the input of a rectifier stage which converts the ac power to dc. Capacitors/inductors and filters are implemented on the dc bus to smooth the voltage/current by filtering harmonics.

The inverter converts dc voltage/current into ac with the desired amplitude and frequency by utilizing PWM techniques controlled by switching signals from the controller, which

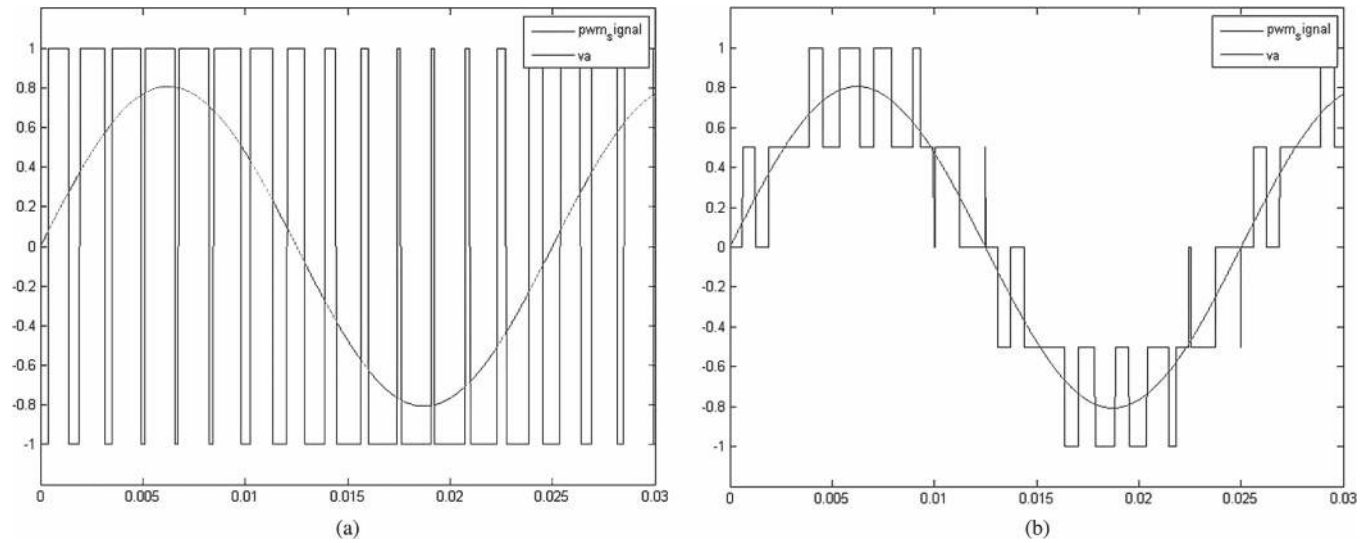

Fig. 3. PWM signals for two- and five-level inverters. (a) Two-level inverter. (b) Five-level inverter.

determines the trigger sequence and time intervals based on the control algorithm.

The conventional type of PWM inverter is a two-level inverter, which has two voltage levels and six switches for three arms (see Fig. 2). The output is a square waveform as shown in Fig. 3(a) with one high voltage level and one low voltage level. The approach for avoiding some of the harmonics of the two-level inverter is to employ a multilevel PWM inverter, which has multiple voltage levels and more accurately approximates a sine wave as illustrated in Fig. 3(b). The THD is reduced by using multilevel inverters [14], [15], where THD is the ratio of the sum of all higher harmonic amplitudes to the fundamental frequency power amplitude when the input is an ideal sine wave

$$\text{THD} = \sqrt{V_2^2 + V_3^2 + \cdots + V_n^2}/V_1. \tag{10}$$

Both the two-level and multilevel inverters "chop" the input dc voltage at a high frequency. The chopped voltage/current signal contains many high frequency harmonics which interact with the motor fundamental frequency, resulting in relatively low frequency torque harmonics as given in [16]

$$f_T = |m \cdot f_{\text{PWM}} \pm n \cdot f_e| \tag{11}$$

where m and n are integers such that

$$(1)\ \begin{cases} m = 0 \\ n = 6j, \quad \forall\, j = 1, 2, 3, \ldots \end{cases}$$

$$(2)\ \begin{cases} m = 2i, \quad \forall\, i = 1, 2, 3, \ldots \\ n = 3(2j), \quad \forall\, j = 0, 1, 2, \ldots \end{cases}$$

$$(3)\ \begin{cases} m = 2i + 1, \quad \forall\, i = 0, 1, 2, \ldots \\ n = 3(2j + 1), \quad \forall\, j = 0, 1, 2, \ldots \end{cases}.$$

The frequencies provided by these formulas appear in the numerical example's torques provided later in this paper. A resonance is said to occur if one of these torque frequencies coincides with a mechanical natural frequency. The torsional motion and stress amplitudes at resonance depend on the amplitude of the corresponding torque harmonic, its proximity to the natural frequency, and the damping of the vibration mode in resonance. Severe vibration and possible failure may result even if the torque harmonic amplitude at the resonance frequency is low when the damping is very light, so users and manufacturers employ couplings that add damping.

For the sake of illustration and because of their widespread usage, only voltage source inverters (VSIs) with open-loop volt/hertz method are considered here. In addition to the torque harmonic due to the PWM, other torque harmonics induced by VSI are discussed in [5], including the effect of deadtime compensation based on current measurement, asymmetric deadtime voltage, and magnetic saturation.

B. Mechanical System

A mechanical system is composed of inertias, shafts, couplings, bearings, gears, etc. In this paper, the machinery train is modeled with lumped masses at n nodes and with $n-1$ beam elements that connect the nodes. Each element between two neighboring nodes is modeled with a stiffness and a damping. The gears are considered as rigid teeth for the torsional motion model. There is only one degree of freedom (DOF) θ_i on each node if only torsional motion is considered, where i indicates the node number.

The inertia matrix for a n node model without gears is

$$I = \begin{bmatrix} I_1 & & & \underline{0} \\ & I_2 & & \\ & & \ddots & \\ \underline{0} & & & I_n \end{bmatrix} \tag{12}$$

where I_i is the lumped inertia at the ith node.

The shaft element stiffness matrix and damping matrix connecting two nodes are given by

$$K_{i,i+1} = \begin{bmatrix} k_{i,i+1} & -k_{i,i+1} \\ -k_{i,i+1} & k_{i,i+1} \end{bmatrix} \tag{13}$$

$$C_{i,i+1} = \begin{bmatrix} c_{i,i+1} & -c_{i,i+1} \\ -c_{i,i+1} & c_{i,i+1} \end{bmatrix} \tag{14}$$

where $k_{i,i+1}$ and $c_{i,i+1}$ are the stiffness and damping between node i and $i+1$, respectively.

The shaft element stiffness connecting nodes i and $i+1$ is

$$k_{i,i+1} = \frac{G_{i,i+1} J_{i,i+1}}{L_{i,i+1}} \tag{15}$$

where G is the shear modulus of the element, L is the length of the element, and J is the torsion constant.

The system stiffness and damping matrix is assembled from $k_{i,i+1}$, $c_{i,i+1}$, and bearing damping at each node

$$\underset{n\times n}{\underline{K}} = \begin{bmatrix} k_{1,2} & -k_{1,2} & 0 & \cdots & 0 \\ -k_{1,2} & k_{1,2}+k_{2,3} & -k_{2,3} & & \\ 0 & -k_{2,3} & k_{2,3}+k_{3,4} & & \\ \vdots & & & \ddots & \vdots \\ 0 & & & \cdots & k_{n-1,n} \end{bmatrix} \tag{16}$$

$$\underset{n\times n}{\underline{C}_s} = \begin{bmatrix} c_{1,2} & -c_{1,2} & 0 & \cdots & 0 \\ -c_{1,2} & c_{1,2}+c_{2,3} & -c_{2,3} & & \\ 0 & -c_{2,3} & c_{2,3}+c_{3,4} & & \\ \vdots & & & \ddots & \vdots \\ 0 & & & \cdots & c_{n-1,n} \end{bmatrix} \tag{17}$$

$$\underset{n\times n}{\underline{C}_b} = \begin{bmatrix} c_1^b & 0 & 0 & & \\ 0 & c_2^b & 0 & & \\ 0 & 0 & c_3^b & & \\ & & & \ddots & \vdots \\ 0 & & & \cdots & c_n^b \end{bmatrix} \tag{18}$$

where c_i^b is the bearing damping of node i.

The external torque applied to the system is

$$\underset{n\times 1}{\underline{T}} = \begin{bmatrix} T_1 \\ \vdots \\ T_n \end{bmatrix}. \tag{19}$$

The complete mechanical system equation of motion is

$$\underset{n\times n}{\underline{I}}\ \underset{n\times 1}{\ddot{\underline{\theta}}} + \left(\underset{n\times n}{\underline{C}_s} + \underset{n\times n}{\underline{C}_b}\right) \underset{n\times 1}{\dot{\underline{\theta}}} + \underset{n\times n}{\underline{K}}\ \underset{n\times 1}{\underline{\theta}} = \underset{n\times 1}{\underline{T}}\,. \tag{20}$$

For a system with n nodes and m set of gears, the system has $n-m$ DOFs since a gear set adds a motion constraint between the driver gear and the follower. The system state mass, stiffness, and damping matrices can be easily derived with a gear ratio transform. Details are provided in [18].

Note that the gear can induce torsional vibration at the frequency of the number of the gear tooth times the rotating speed. This is critical when considering premature tooth wear. However, this paper only focuses on the resonance of lower shafting-related modes.

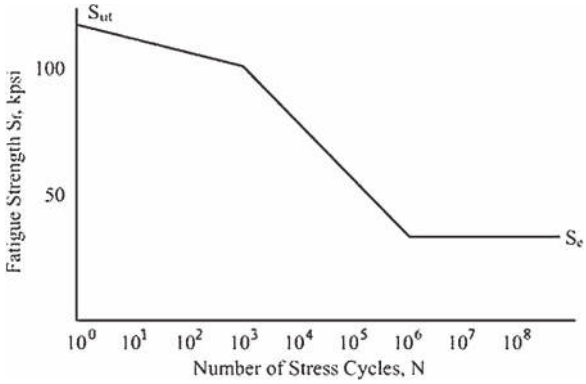

Fig. 4. Typical S–N curve.

C. Torsional Fatigue and Life Prediction

1) S–N Curve: The cyclic stress–life relation for ductile materials undergoing cyclic constant amplitude stress is typically described by an S–N curve [19], as shown in Fig. 4.

The S–N curve is typically expressed in the form shown in Fig. 4, where S_f is the cyclic stress amplitude, N is the number of cycles to failure, and the constants a and b are typically defined from the $N = 10^3$ and $N = 10^4$ points as

$$a = (fS_{ut})^2/S_e \tag{21}$$

$$b = -1/3 \log(fS_{ut}/S_e) \tag{22}$$

where f is the fatigue strength fraction, S_{ut} is the ultimate stress, and S_e is the endurance limit.

Then, the number of cycles to failure can be calculated from

$$N = (\sigma_a/a)^{1/b} \tag{23}$$

where σ_a is the alternating stress amplitude.

2) Effective Shear Stress: The combination of mean and alternating stresses requires the definition of an effective stress for determining fatigue life by using the S–N curves. The shear stress in a shaft or coupling due to pure torsional loading is given by

$$\tau = T_{\text{trans}} \cdot r_{\text{outer}}/J \tag{24}$$

$$J = \pi/2 \left(r_{\text{outer}}^4 - r_{\text{inner}}^4\right) \tag{25}$$

where τ is the shear stress, T_{trans} is the transmitted torque through the coupling/shaft, r_{outer} is the outer radius of the coupling/shaft, r_{inner} is the inner radius of the coupling/shaft, and J is the torsion constant.

Wang [19] states that: *"Experimental results tend to show that the value of the mean shear stress has no influence on the fatigue life of a ductile structural component subjected to cyclic torsional loading as long as the maximum stress is less than the yield strength of the material. Shigley and Mitchell stated 'up to a certain point, torsional mean stress has no effect on the torsional endurance limit'. Hence, the plot of the alternating shear stress τ_a versus mean shear stress τ_m bound by a horizontal line with $\tau_a = \tau_e$ and a 45 deg yield line."* This is illustrated in Fig. 5.

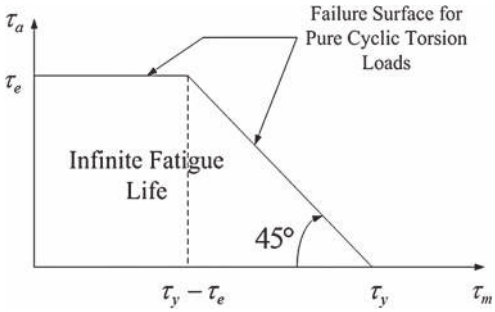

Fig. 5. Pure torsion load criterion, where τ_e is the endurance limit, τ_y is the torsional yield strength, τ_m is the mean stress, and τ_a is the alternating stress.

Loss of life occurs for a fluctuating pure torsional load with τ_m and τ_a when either

$$\tau_m < \tau_y - \tau_e \text{ and } \tau_a > \tau_e$$

$$\Rightarrow \tau_{\text{eff}} = \tau_a \text{ (mean stress has no influence) or}$$

$$\tau_m > \tau_y - \tau_e \text{ and } \tau_a > \tau_y - \tau_m$$

$$\Rightarrow \tau_{\text{eff}} = \frac{\tau_a}{\left(\frac{\tau_y - \tau_m}{\tau_e}\right)} \text{ (mean stress has influence).}$$

Endurance limit τ_e values provided in the reference literature typically correspond to highly polished "ideal" specimens. The reduction in endurance limit due to manufacturing, installation, loading, and environmental conditions is accounted for by multiplying the ideal endurance limit by so-called Marin factors [20], as expressed by

$$\tau_e' = \tau_e \times k_a \times k_b \times k_c \times k_d \times k_e \times k_f \tag{26}$$

where $k_a = 1.58 \times S_{ut}^{-0.086}$ is the surface factor using ground finish (S_{ut} in megapascals); $k_b = 1.24 \times d^{-0.107} (2.79 < d < 51)$ or $1.51 \times d^{-0.157} (51 < d < 254)$ is the size factor, where d is the shaft diameter in millimeters; $k_c = 0.577$ is the loading factor for torsion; $k_d = 1$ is the temperature factor for 20 °C; $k_e = 0.897$ is the reliability factor for 90% reliability; and $k_f = 1$ is the miscellaneous effect factor.

The effective shear stress should be multiplied by a stress concentration factor if geometric discontinuities, such as keyways, occur along the shaft [20].

3) Varying Fluctuating Stress and Rain-Flow Algorithm: Usage of the aforementioned approaches assumes constant values for the mean stress τ_m and alternating stress τ_a. The rain-flow algorithm is utilized for the case that τ_m and τ_a vary with time, e.g., during a machinery train start-up.

The rain-flow algorithm decomposes a varying fluctuating stress load into a series of simple stress load reversals, which have constant τ_m and τ_a (for details, please refer to [21]–[23]). Then, the accumulated damage D can be derived by Miner's rule by obtaining the number of cycles for each simple stress level

$$D = \sum \frac{n_i}{N_i} \tag{27}$$

where n_i is the number of cycles obtained from the rain-flow algorithm for the ith stress amplitude reversal level and N_i is the number of cycles to failure for the ith stress reversal obtained from an S–N curve. Failure is estimated to occur when D exceeds 1, so $1/D$ indicates how many times the original stress load can be applied before failure.

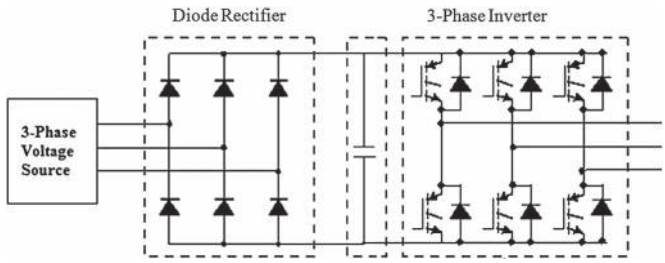

Fig. 6. Example electrical system.

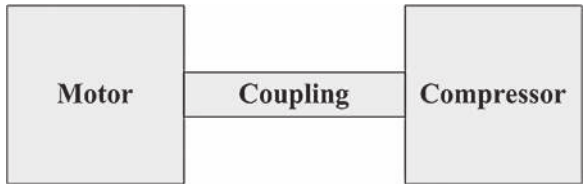

Fig. 7. Example mechanical system.

TABLE I
MOTOR ELECTRICAL PARAMETERS

Nominal Power	200 HP (149 kW)
Nominal Voltage	460 V
Nominal Frequency	60 Hz
Stator Resistance	0.01818 ohm
Stator Leakage Inductance	0.00019 H
Rotor Resistance	0.009956 ohm
Rotor Leakage Inductance	0.00019 H
Mutual Inductance	0.009415 H
Number of Poles	4

TABLE II
SYSTEM MECHANICAL PARAMETERS

Motor Inertia	2.6 kg.m^2
Motor Bearing Damping	0.04789 N.m/(rad/s)
Compressor Inertia	2.5 kg.m^2
Compressor Bearing Damping	0 N.m/(rad/s)
Coupling Stiffness	6.9781e4 N.m/rad
Coupling Damping	10 N.m/(rad/s)
Coupling Length	0.2667 m
Coupling Radius (outer/inner)	0.0254 m / 0.02286 m
Coupling Shear Modulus	8.27e10 N/m^2

D. Coupled Electrical/Mechanical System

The electrical and mechanical systems are coupled at the motor rotor. The electrical subsystem generates electromagnetic torque, which is the input to the mechanical subsystem. For the sake of illustration, MATLAB SimPowerSystems is used to model the electrical system, including the three-phase voltage source, rectifier, inverter, and motor, while the mechanical system is modeled in state-space form and implemented via the Simulink State-Space block. The electromagnetic torque of the motor output is one of the inputs to the mechanical state-space block (the other input is the mechanical load torque).

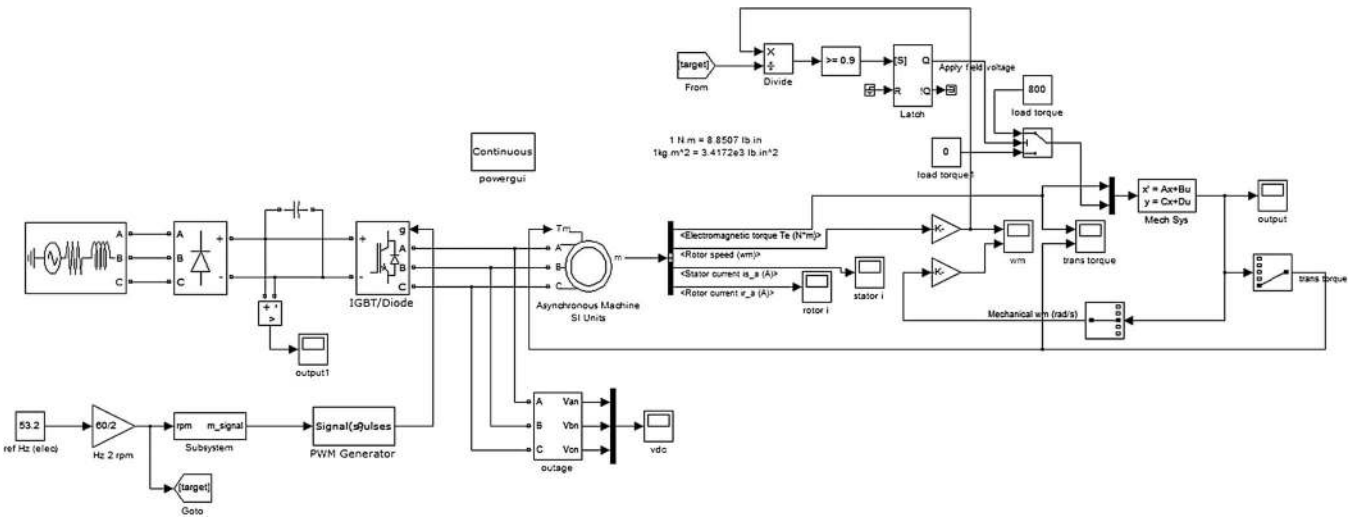

Fig. 8. Model block diagram.

Damping and stiffness torques occur along the shafting at couplings, shaft segments, and bearings. For example, the flange or coupling torque has the following general form, is calculated in the mechanical state-space model, and is fed back to the motor block in SimPowerSystems:

$$T_c = k_c(\theta_1 - \theta_2) + b_c(\omega_1 - \omega_2) \tag{28}$$

where T_c is the transmitted torque through motor coupling, k_c is the coupling stiffness, b_c is the coupling damping, $\theta_1 - \theta_2$ is the relative angular displacement of the two ends of the coupling, and $\omega_1 - \omega_2$ is the relative angular velocity of the two ends of the coupling.

The motor rotor inertia is modeled twice, once in the motor model of SimPowerSystems and once in the mechanical state-space model. These two inertia models are subjected to the same drive torque and drag torque and have exactly the same torsional motion. The effects of motor rotor lateral motion on internal magnetic fields and forces are neglected for the sake of simplicity.

IV. Simulation Verification for Steady-State Resonance

A simple mechanical machinery train with two inertias is simulated to illustrate resonance vibration due to VFD. The system includes a simple open-loop volt/hertz control method and only pure torsional motions. The prediction of system life for the case of resonance response is considered.

A. System Description

1) Electrical System: The power electronic system shown in Fig. 6 includes six diodes in the rectifier circuit that rectifies the input three-phase voltage into a dc voltage, a capacitor to smooth the dc bus link to supply a constant dc voltage, and a three-arm two-level inverter composed by six IGBTs.

The switching signal is generated by a carrier-based PWM, which compares the triangular carrier signal with the sinusoidal modulation signal. The magnitude of the sinusoidal modulation signal is proportional to the electrical frequency to keep a constant volt/hertz ratio.

2) Mechanical System: The mechanical system shown in Fig. 7 represents a simple two-mass system with a compressor driven by a motor. The motor electrical parameters and system mechanical parameters are listed in Tables I and II, respectively. The system's undamped natural frequency is 37.24 Hz, and the damped natural frequency is 37.23 Hz. The constant load acting on the compressor is 800 N · m, and the mean coupling shear stress is about 9.032e7 N/m^2.

TABLE III
Power Electronic Device Settings

Rectifier Diodes	
Forward Voltage	0 V
Internal Resistance	1e-3 ohm
DC Bus Capacitor	
Capacitance	0.5 F
Inverter IGBTs	
Forward Voltage	0.8 V
Internal Resistance	1e-3 ohm
Fall Time	1e-6 sec
Tail Time	2e-6 sec
Clamped Diode Forward Voltage	0.8 V

B. Modeling

The entire system is modeled using MATLAB SimPowerSystems and Simulink. The model block diagram shown in Fig. 8 includes the mechanical system modeled in state-space form as a Simulink block and the electrical components modeled with SimPowerSystems blocks. The parameter values of the power electronic devices are listed in Table III.

C. Torque Harmonic Verification

The motor input voltage frequency is set to 60 Hz (electrical frequency), which determines the mechanical spin speed which is approximately 30 Hz. The PWM carrier frequency is held constant at 1080 Hz. The resultant motor speed, electromagnetic torque spectrums, coupling shear stress, and shear

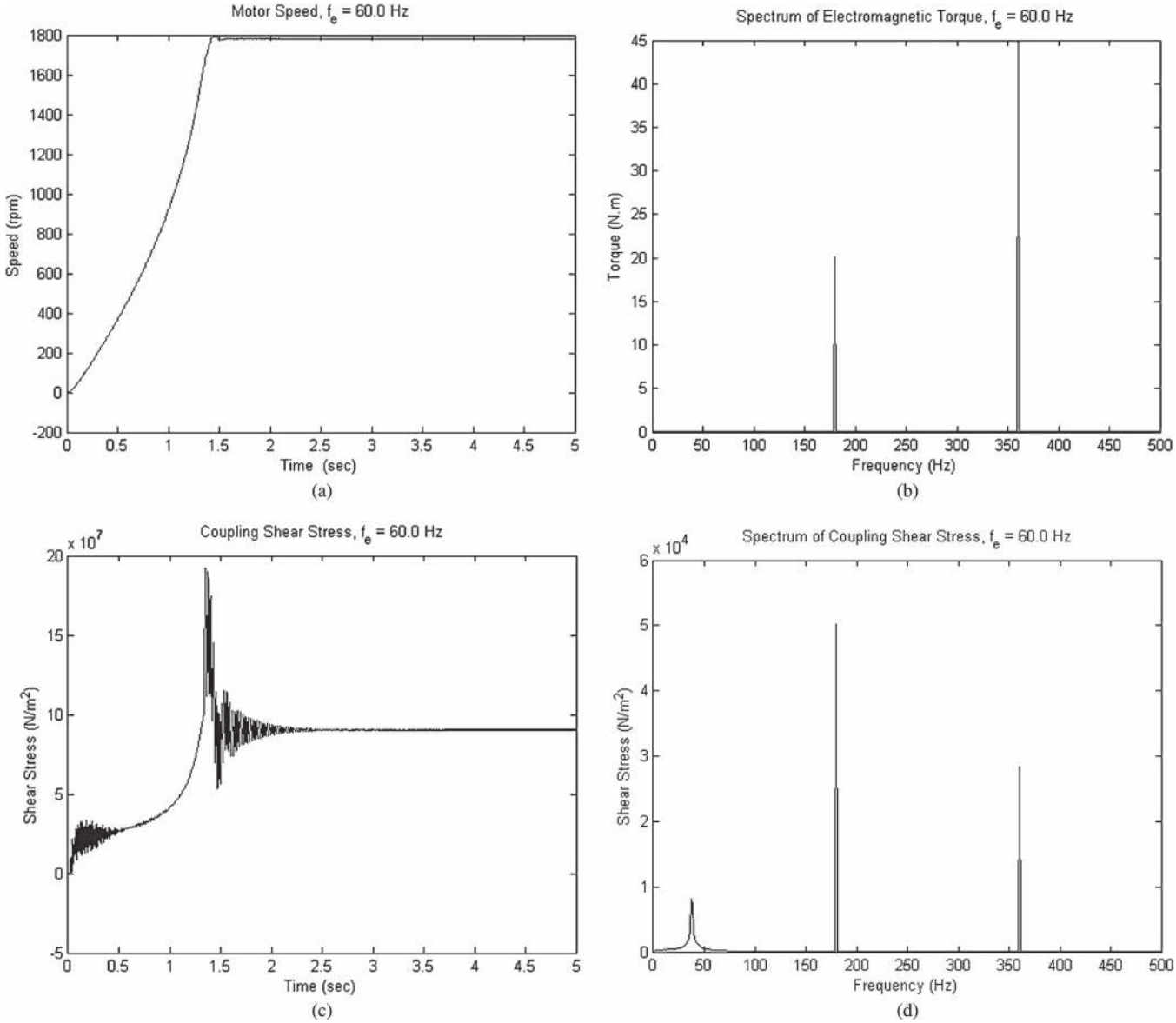

Fig. 9. $f_e = 60$ Hz simulation results. (a) Motor speed. (b) Torque spectrum. (c) Coupling shear stress. (d) Shear stress spectrum.

stress spectrums are shown in Fig. 9. The harmonic frequencies match the theoretical formula described in [16]. For the 60-Hz case, $f_e = 60$ Hz, and $f_{\rm pwm} = 1080$ Hz. By (12), $f_T = 180, 360, 540 \ldots$ Hz.

Fig. 10 shows an interference plot with the torque harmonics based on (12) with $f_{\rm pwm} = 1080$ Hz. The horizontal axis indicates the electrical frequency, while the vertical axis presents the torque harmonic frequency. The horizontal line indicates the system natural frequency of 37.24 Hz. The intersecting points are possible resonance points where the torque harmonic coincides with the system natural frequency.

Fig. 11 shows responses for an electrical frequency of 53.2 Hz, which clearly indicates a resonance condition. The torque spectrum shows a harmonic component at 37.2 Hz which is very close to the system natural frequency of 37.23 Hz. The shear stress zero-peak alternating component is approximately 1.004e7 N/m^2 at steady state, which far exceeds its counterpart stress at the electrical frequencies of 60 Hz, indicating the occurrence of a resonance. Clearly, the magnitude (6.067 N $\cdot$ m,

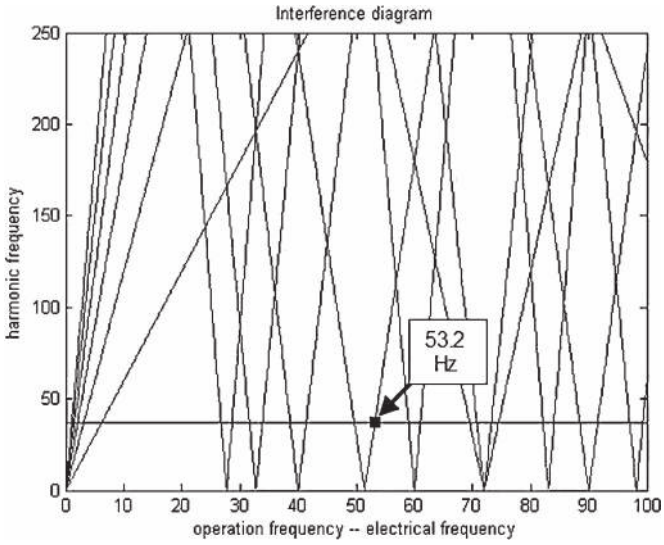

Fig. 10. Interference diagram for $f_{\rm pwm} = 1080$ Hz.

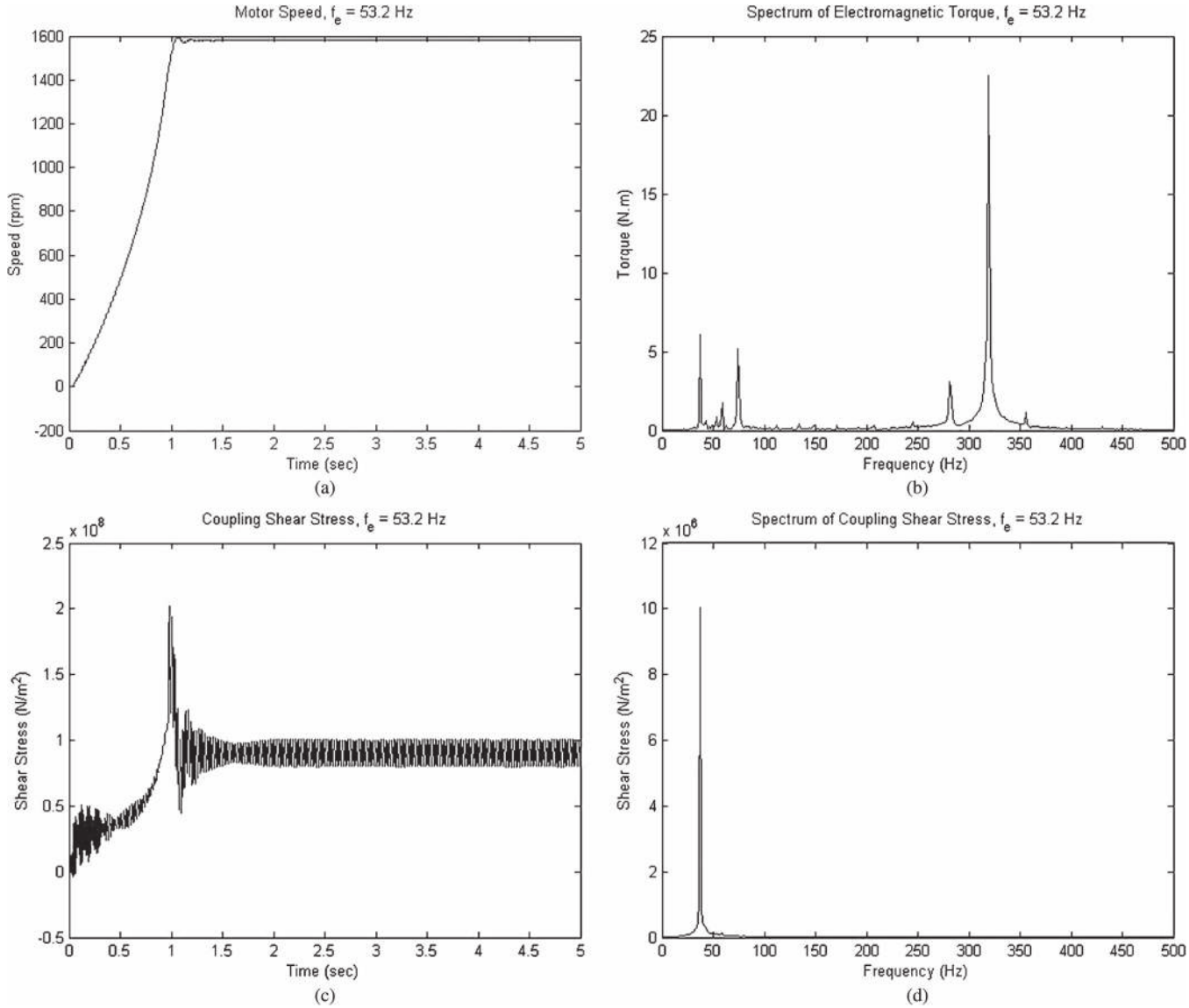

Fig. 11. $f_e = 53.2$ Hz simulation results. (a) Motor speed. (b) Torque spectrum. (c) Coupling shear stress. (d) Shear stress spectrum.

zero-peak) of the 37.2 Hz torque harmonic in Fig. 11(b) is smaller than other ones, i.e., at 320 Hz (22.48 N · m, zero-peak). However, the shear stress spectrum in Fig. 11(d) shows a strong dominance of the 37.2 Hz component, supporting the evidence of resonance. This supports the assertion in [16] that the frequency of a torque harmonic has much greater importance than its magnitude.

D. Life Prediction

Large shear stresses that result from the resonant operation of machinery may significantly reduce shaft or coupling life even after a relatively short duration. The S–N curve and rain-flow algorithm are employed to provide a quantitative estimate of the life reduction and estimated time to failure, as discussed earlier. The coupling material specifications are listed in Table IV for this example.

The torsional stress specifications are obtained from the following equations [24], [25] relating tensile and torsional strength:

TABLE IV
COUPLING TENSILE SPECIFICATION

Coupling Tensile Ultimate Strength S_{ut}	1.11e9 N/m^2
Coupling Tensile Yield Strength S_y	71e7 N/m^2
Coupling Fatigue Strength Exponent b	-0.091
Surface Factor k_a	0.87
Size Factor k_b	0.8162
Loading Factor k_c	0.577
Temperature Factor k_d	1
Reliability Factor k_e	0.897
Miscellaneous Effects Factor k_f	1
Keyway Concentration Factor	3

$$\text{Torsional Endurance Limit } \tau_e = S_{ut}/25 \tag{29}$$

$$\text{Torsional Yield Strength } \tau_y = 0.55 S_y. \tag{30}$$

Resonance life prediction is based on the shear stress record between $t = 4$ s and $t = 5$ s in Fig. 11(c). Failure is predicted

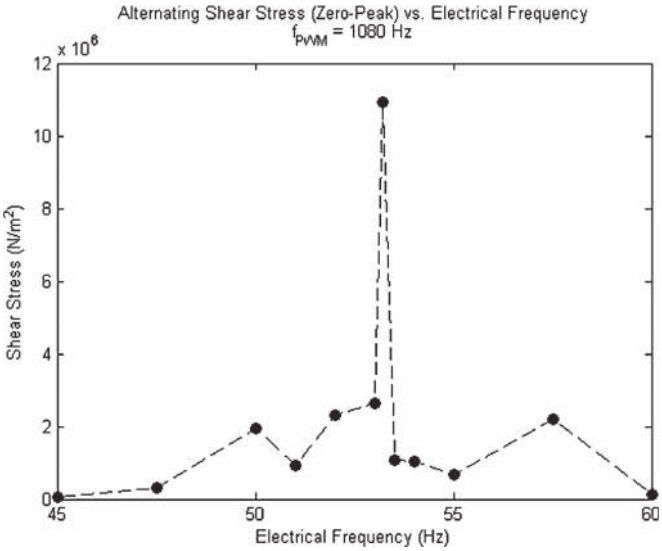

Fig. 12. Alternating shear stress versus electrical frequency with $f_{\mathrm{pwm}} = 1080$ Hz and $f_e = 45 \sim 60$ Hz.

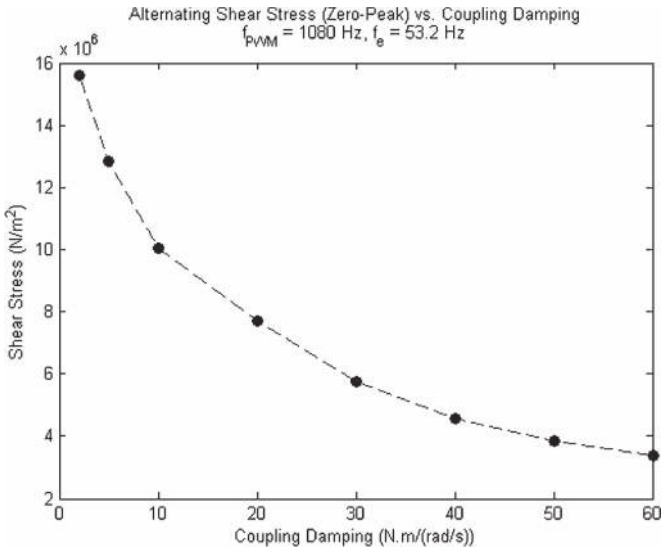

Fig. 13. Alternating shear stress versus coupling damping with $f_e = 53.2$ Hz and $f_{\mathrm{pwm}} = 1080$ Hz.

TABLE V
ALTERNATING SHEAR STRESS AND PREDICTED LIFE VERSUS ELECTRICAL FREQUENCY WITH $f_{\mathrm{pwm}} = 1080$ Hz AND MEAN SHEAR STRESS OF 9.032e7 N/m^2

Electrical Frequency f_e (Hz)	Alternating Steady State Shear Stress Zero-Peak (N/m^2)	Steady State Operation Time before Failure (sec)
45	0.71e5	Inf
50	19.37e5	Inf
53	26.27e5	Inf
53.2	100.4e5	46.0505
53.5	10.57e5	Inf
55	6.79e5	Inf
60	1.36e5	Inf

TABLE VI
ALTERNATING SHEAR STRESS AND PREDICTED LIFE VERSUS ELECTRICAL FREQUENCY WITH $f_e = 53.2$ Hz, $f_{\mathrm{pwm}} = 1080$ Hz, AND MEAN SHEAR STRESS OF 9.032e7 N/m^2

Coupling Damping (N.m.s)	Alternating Steady State Shear Stress Zero-Peak (N/m^2)	Steady State Operation Time before Failure (sec)
2	15.6e6	2.8048
5	12.8e6	4.9824
10	10.04e6	46.0505
20	7.72e6	1.7631e3
30	5.74e6	5.6029e5
40	4.58e6	Inf
60	3.36e6	Inf

to occur after 46.05 repetitions of this operation cycle, which, in this case, is a very short duration: 46.05 s.

Fig. 12 and Table V show the effect of varying the electrical frequency on alternating shear stress and life, with the PWM switching frequency maintained at 1080 Hz for all cases. Fig. 12 should not be interpreted as a standard frequency response plot as utilized in control modeling or resonance studies since the electrical frequency is not the excitation frequency but instead changes the excitation frequency according to (12) and Fig. 10.

Fig. 13 and Table VI show the effect of coupling damping on alternating shear stress and coupling life. With increased coupling damping, the shear stress is seen to be significantly reduced, and life is seen to be significantly increased. This represents a common remedy for torsional shear stress-induced high-cycle fatigue failures in machinery.

E. Simulation With Multilevel Inverters

1) Resonance Case $f_e = 53.2$ Hz: A comparison between the three- and five-level inverter approaches is made for the resonance case, where $f_e = 53.2$ Hz.

The simulation results are shown in Figs. 14 and 15 for three- and five-level inverter approaches, respectively. The five-level inverter shear stress responses are smaller than the three-level one but are still significant at resonance.

A comparison of the steady-state torque, resonance alternating shear stress component, and steady-state operation time before failure between two-, three-, and five-level inverter systems is shown in Table VII. The mean shear stress is approximately 9.032e7 N/m^2.

Note that, although the overall peak–peak steady-state torque pulsation magnitude decreases as the number of the inverter level increases, the torque component near the resonance frequency may increase. This explains why the three-level inverter shear stress is much larger than the two-level inverter shear stress. The five-level inverter shear stress is less than the three-level inverter shear stress but is larger than the two-level inverter shear stress.

The reason for this is explained based on the torque–current relationship developed in [16] with the assumption that it is dominated by large dc components. As stated in [16], the torque harmonic frequencies and current harmonic frequencies can be written as

$$f_\tau = |m \cdot f_{\mathrm{PWM}} \pm n \cdot f_e| \tag{31}$$
$$f_c = |x \cdot f_{\mathrm{PWM}} \pm y \cdot f_e| \tag{32}$$
$$x = m, y = n \pm 1 \tag{33}$$

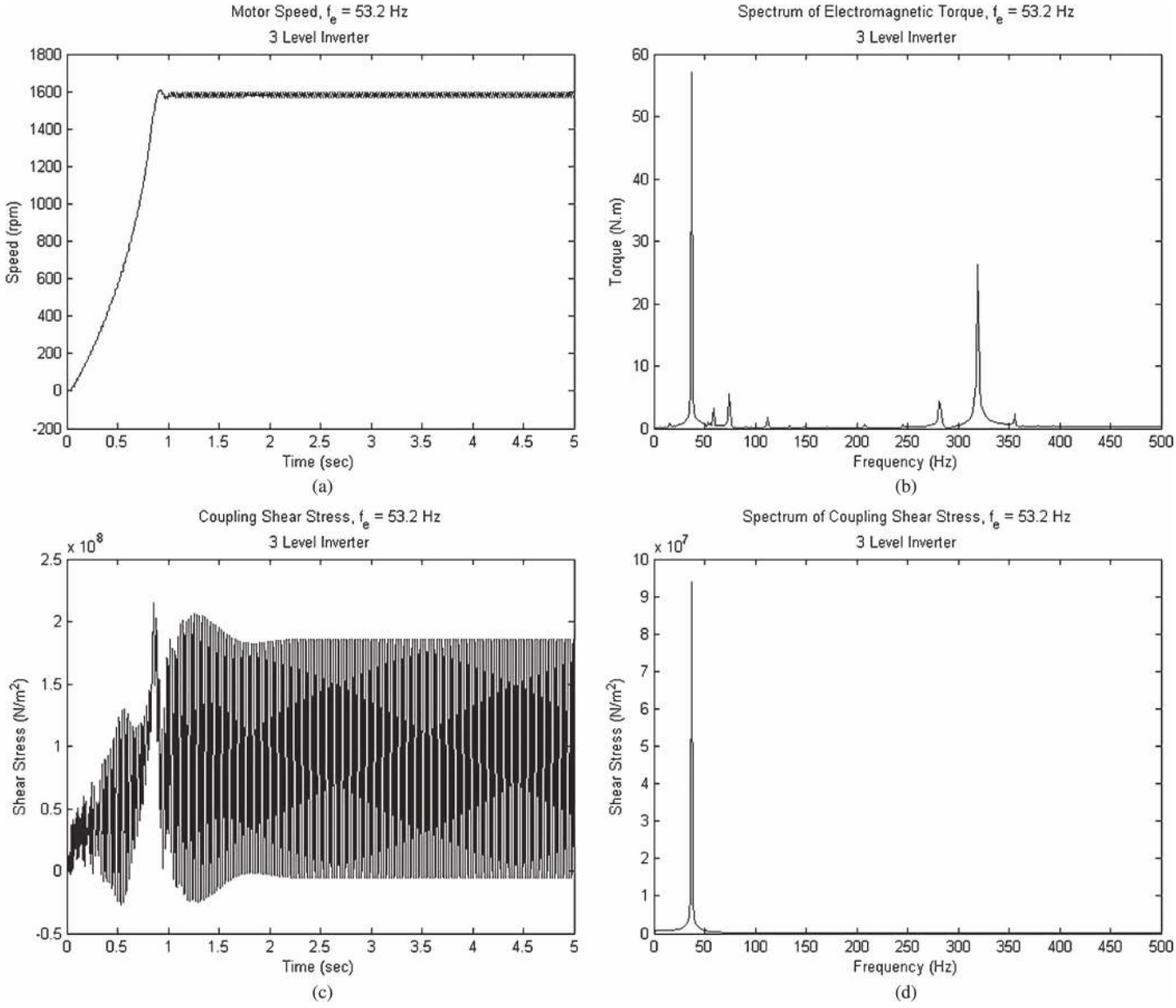

Fig. 14. $f_e = 53.2$ Hz three-level inverter simulation results. (a) Motor speed. (b) Torque spectrum. (c) Coupling shear stress. (d) Shear stress spectrum.

where

$$(1)\begin{cases} m = 0 \\ n = 6j, \quad \forall j = 1, 2, 3. \ldots \end{cases}$$

$$(2)\begin{cases} m = 2i, \qquad \forall i = 1, 2, 3, \ldots \\ n = 3(2j), \quad \forall j = 0, 1, 2, \ldots \end{cases}$$

$$(3)\begin{cases} m = 2i + 1, \qquad \forall i = 0, 1, 2, \ldots \\ n = 3(2i + 1), \quad \forall j = 0, 1, 2, \ldots . \end{cases}$$

The resonance frequency is 37.2 Hz, where $f_{\mathrm{pwm}} = 1080$ Hz and $f_e = 53.2$ Hz. The corresponding m and n values for $f_T = 37.2$ Hz are

$$m = 1, \quad n = 21. \tag{34}$$

The current harmonics that cause the resonance inducing torque harmonic at 37.2 Hz are those at 16.0, 90.4, 2144, and 2250.4 Hz and are calculated by

$$x = 1, y = 21 \pm 1 = \begin{cases} 20 \\ 22 \end{cases} \tag{35}$$

$$f_c = |x \cdot f_{\mathrm{PWM}} \pm y \cdot f_e| = \begin{cases} |1 \cdot f_{\mathrm{PWM}} \pm 20 \cdot f_e| \\ |1 \cdot f_{\mathrm{PWM}} \cdot f_e| \, . \end{cases} \tag{36}$$

Vibrations and stresses are caused by torques which are, in turn, caused by currents. The currents result from voltages, and therefore, the cause of the vibration may be understood by considering voltages. The voltage harmonics at 16.0, 90.4, 2144, and 2250.4 Hz are compared for the two-, three-, and five-level inverter cases, as shown in Fig. 16.

The spectrum clearly shows that the voltage harmonic magnitudes at 16.0, 90.4, 2144, and 2250.4 Hz increase as the inverter level changes from two, to five, and to three. The bigger the voltage harmonic, the bigger the current harmonic, and the bigger the corresponding torque harmonic component at 37.2 Hz. Thus, the torque harmonic at 37.2 Hz increases

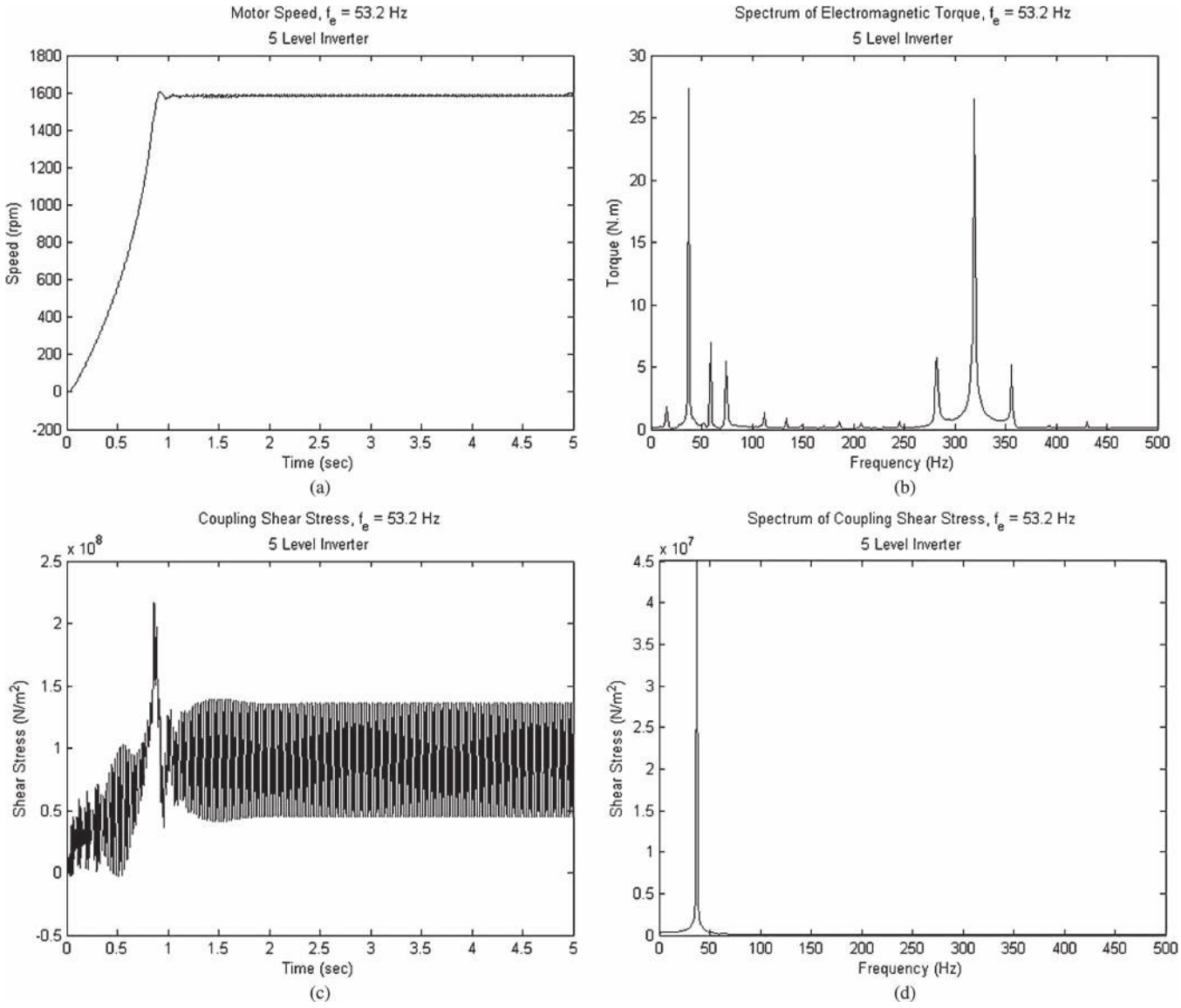

Fig. 15. $f_e = 53.2$ Hz five-level inverter simulation results. (a) Motor speed. (b) Torque spectrum. (c) Coupling shear stress. (d) Shear stress spectrum.

TABLE VII
COMPARISON OF STEADY-STATE ALTERNATING SHEAR STRESS FOR TWO-, THREE-, AND FIVE-LEVEL SYSTEMS WITH $f_e = 53.2$ Hz

No. of Inverter Levels	Motor Input Voltage THD Phase-Neutral (%)	Alternating Motor Torque zero-peak (N.m)	Motor Torque at Resonance Freq. zero-peak (N.m)	Alternating Shear Stress at Resonance Freq. zero-peak (N/m^2)	Steady State Operation Time before Failure (sec)
2-level	63.42	251.8	6.067	1.004e7	46.0505
3-level	32.65	246.7	57.14	9.406e7	<1
5-level	16.41	134.7	27.36	4.497e7	<1

as the inverter level changes from two, to five, and to three. This and the presence of the mechanical natural frequency at 37.2 Hz explain why the vibration and stress increase as the inverter level changes from two, to five, and to three. This result is consistent with the theory presented in [16] which provides formulas for related current and torque harmonic frequencies.

The resonance shear stress can be significantly reduced by changing the PWM switching frequency as illustrated for the case shown in Fig. 17 where the five-level inverter $f_{\rm pwm}$ is increased from 1080 to 1090 Hz while maintaining the electrical frequency $f_e = 53.2$ Hz. This causes the total alternating shear stress to reduce from 4.497e7 N/m^2 zero-peak to 2.997e6 N/m^2, and the steady-state operation time before failure increases from less than 1 s to infinity. Care should be taken in using this approach though since the new $f_{\rm pwm}$ may produce torque harmonics that cause resonance at some other f_e.

V. CONCLUSION

The major contributions of this paper include the following.

1) A systematic approach for evaluating the fatigue life of a complex machinery train powered by a VFD motor and undergoing torsional vibration. A realistic model is utilized, including detailed power electronics, motor, gears, couplings, and shaft components. Life prediction is based

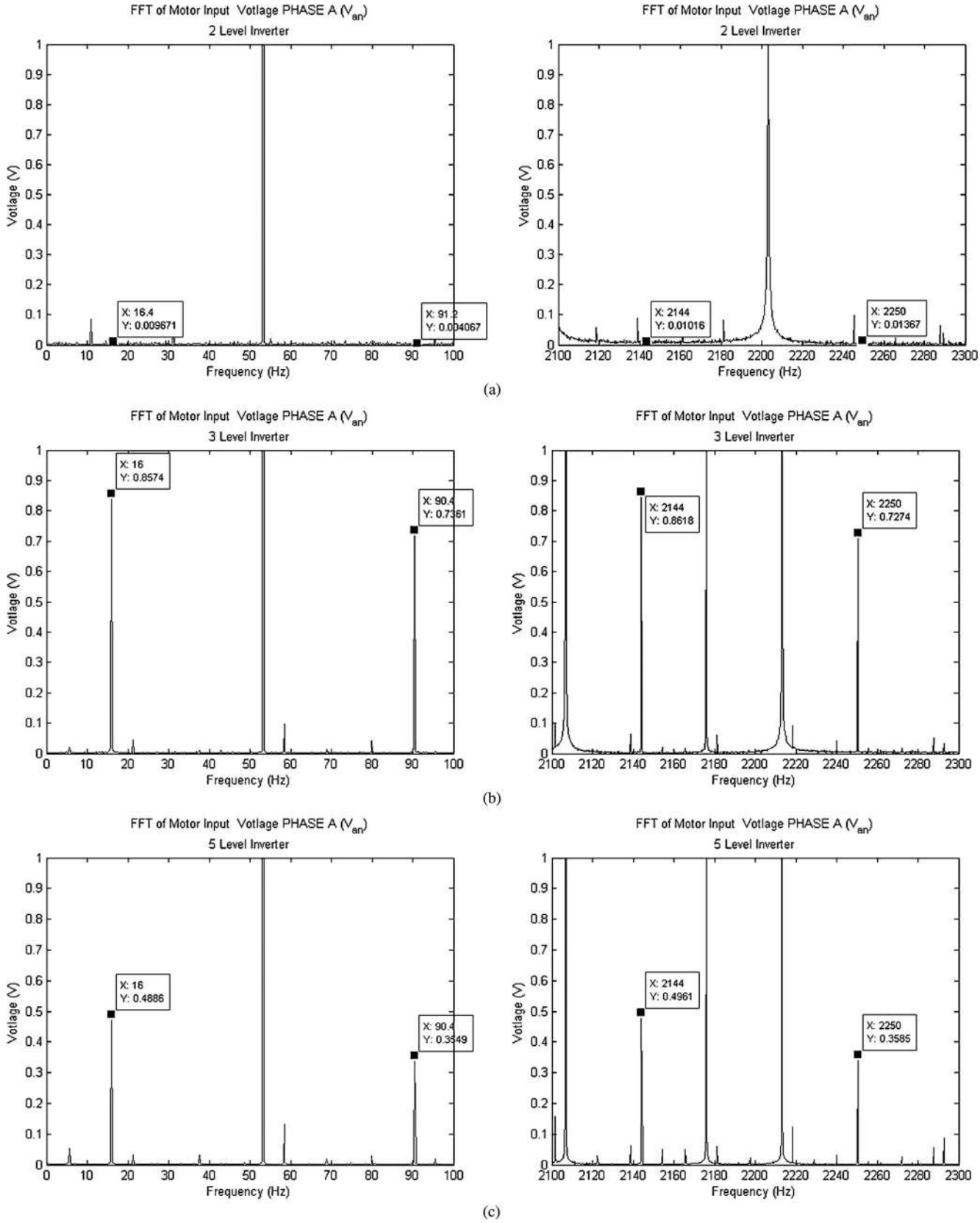

Fig. 16. Comparison of voltage harmonics at 16.0, 90.4, 2144, and 2250.4 Hz with $f_e = 53.2$ Hz and $f_{\rm pwm} = 1080$ Hz. (a) Two-level inverter. (b) Three-level inverter. (c) Five-level inverter.

on the rain-flow approach which is applicable to transient start-up events and to sustained steady-state cyclic stress related to resonance. Prior approaches in the literature are too restrictive in assuming that all resonances will cause failure and also do not provide a means to estimate life.

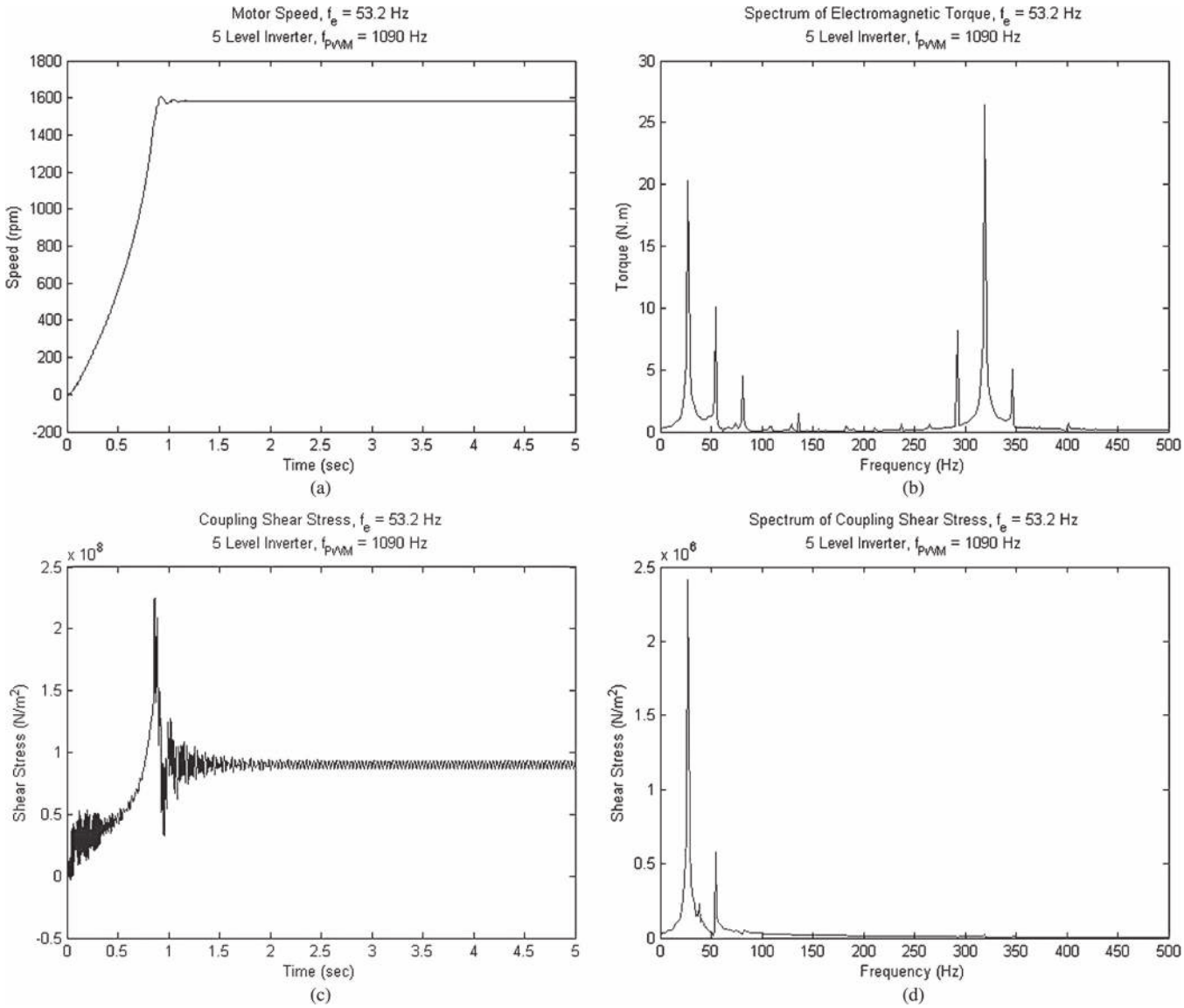

Fig. 17. Simulation results for five-level inverter with $f_e = 53.2$ Hz and $f_{\rm pwm} = 1090$ Hz. (a) Motor speed. (b) Torque spectrum. (c) Coupling shear stress. (d) Shear stress spectrum.

2) Demonstration that, although utilizing higher level inverters will reduce the THD in the motor torque, individual frequency components near resonance frequencies may actually increase in amplitude and exacerbate resonance with higher inverter levels. Prior approaches provide a misconception that reducing THD is sufficient to lower all individual torque component amplitudes.
3) Mitigation of damaging resonance conditions that are not alleviated by utilizing a higher level inverter may be accomplished with a PWM carrier frequency interleaving on a four-thread VFD as demonstrated in [16]. This paper provides the alternative approaches of slight shifting of $f_{\rm pwm}$ or utilizing a coupling with increased damping.

VI. Future Work

Areas of future work include the following: 1) increasing the fidelity of the modeling components, such as including the deadtime voltage due to switching mentioned in [5] and closed-loop drive; 2) improving the mechanical model with torsional–lateral motion coupling; 3) correlation of predictions and experimental verification; and 4) modeling the entire machinery train with the four-thread VFD as mentioned in [16] to eliminate certain selected torque components in the torque spectrum.

Acknowledgment

The authors gratefully acknowledge the support of this research from the Texas A&M Turbomachinery Research Consortium member companies (http://turbolab.tamu.edu/articles/turbomachinery_research_consortium).

References

[1] S. Y. Jung, "A torsional vibration analysis of synchronous motor driven trains by the modal method," College Station, TX, USA, Aug. 1986.
[2] G. L. Godwin and E. F. Merrill, "Oscillatory torques during synchronous motor starting, transactions of industry and general applications," *IEEE Trans. Ind. Gen. Appl.*, vol. IGA-6, no. 3, pp. 258–265, May 1970.

[3] E. D. Goodman and T. H. Barton, "Startup torques in synchronous motor drives," *IEEE Trans. Ind. Appl.*, vol. IA-14, no. 3, pp. 193–198, May 1978.
[4] D. G. Holmes, "A general analysis method for determining the theoretical harmonic components of carrier based PWM strategies," in *Conf. Rec. IEEE IAS Annu. Meeting*, 1998, pp. 1207–1214.
[5] J. Plotkin, U. Schaefer, and R. Hanitsch, "Torque ripple in PWM-VSI-fed drives due to parasitic effects in the inverter control," in *Proc. IEEE Conf. Ind. Electron.*, Nov. 2009, pp. 1368–1372.
[6] D. J. Sheppard, "Torsional vibration resulting from adjustable-frequency ac drives," *IEEE Trans. Ind. Appl.*, vol. 24, no. 5, pp. 812–817, Sep./Oct. 1988.
[7] T. Feese, R. Maxfield, and M. Hilscher, "Torsional vibration problem with motor/ID fan system due to PWM variable frequency drive," in *Proc. 37th Turbomach. Symp.*, 2008, pp. 45–56.
[8] J. C. Wachel and F. R. Szenasi, "Analysis of torsional vibrations in rotating machinery," in *Proc. 22nd Turbomach. Symp.*, 1993, pp. 127–151.
[9] J. A. Kocur, Jr. and J. P. Corcoran, "VFD induced coupling failure," in *Proc. 37th Turbomach. Symp. Case Study*, 2008.
[10] B. Howes, *Perplexing Variable Frequency Drive Vibration Problems*. Calgary, AB, Canada: Beta Machinery Anal. Ltd., 2004.
[11] L. De la Roche and B. Howes, *Lateral and Torsional Vibration Problems in Systems Equipped With Variable Frequency Drives*. Calgary, AB, Canada: Beta Machinery Anal. Ltd., 2005.
[12] R. J. Kerkman, J. Theisen, and K. Shah, "PWM inverters producing torsional components in ac motors," in *Proc. IEEE 55th PCIC*, Cincinnati, OH, USA, 2008, pp. 1–9.
[13] M. Tsukakoshi, M. Al Mamun, K. Hashimuar, H. Hosoda, J. Sakaguchi, and L. Ben-Brahim, "Novel torque ripple minimization control for 25MW variable speed drive system fed by multilevel voltage source inverter," in *Proc. 39th Turbomach. Symp.*, Houston, TX, USA, 2010, pp. 193–200.
[14] M. Ashari, "Practical implementation of multilevel inverter for reducing current on an induction motor bearing," in *Proc. 4th Saudi Tech. Conf. Exhib.*, Riyadh, Saudi Arabia, Dec. 2007.
[15] S. Khomfoi and L. M. Tolbert, *Power Electronics Handbook,* 2nd ed. Amsterdam, The Netherlands: Elsevier, 2007, ch. 17.
[16] J. Song-Manguelle, S. Schröder, T. Geyer, G. Ekemb, and J. Nyobe-Yome, "Prediction of mechanical shaft failures due to pulsating torques of variable-frequency drives," *IEEE Trans. Ind. Appl.*, vol. 46, no. 5, pp. 1979–1988, Sep./Oct. 2010.
[17] D. W. Novotny and T. A. Lipo, *Vector Control and Dynamics of AC Drives*. London, U.K.: Oxford Univ. Press, 1997.
[18] W. J. Chen and E. J. Gunter, *Introduction to Dynamics of Rotor-Bearing Systems*. Bloomington, IN, USA: Trafford, 2005, pp. 367–398.
[19] S. Wang, "Mean shear stress effect for a notch-free ductile material under pure cyclic torsional loads," *ASME J. Pressure Vessel Technol.*, vol. 128, no. 4, pp. 667–669, Jan. 2006.
[20] R. G. Budynas and J. K Nisbett, *Shigley's Mechanical Engineering Design,* 8th ed. New York, NY, USA: McGraw-Hill, 2008.
[21] S. Ariduru, "Fatigue Life Calculation by Rainflow Cycle Counting Method," M.S. thesis, Texas A&M Univ., College Station, TX, USA, 2004.
[22] *Standard Practices for Cycle Counting in Fatigue Analysis*, ASTM E1049-85(2011)e1, 2011.
[23] P. H. Wirsching, T. L. Paez, and K. Ortiz, *Random Vibrations: Theory and Practice*. New York, NY, USA: Dover, 2006.
[24] J. C. Wachel and F. R. Szenasi, "Analysis of torsional vibrations in rotating machinery," in *Proc. 22nd Turbomach. Symp.*, 2003, pp. 127–151.
[25] I. J. Garshelis, R. J. Kari, and S. Bitar, "Magnetic means for determining torsional yield strength," *IEEE Trans. Magn.*, vol. 39, no. 5, pp. 3298–3300, Sep. 2003.

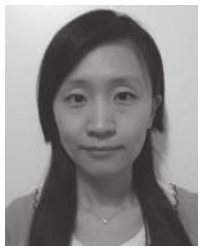

Xu Han received the B.S. degree in electrical engineering from Zhejiang University, Zhejiang, China, in 2008 and the M.S. degree in mechanical engineering from Texas A&M University, College Station, TX, USA, in 2010, where she is currently working toward the Ph.D. degree in mechanical engineering, working on mechanical vibration related to motors and motor drives.

Alan B. Palazzolo received the Ph.D. degree from the University of Virginia, Charlottesville, VA, USA, in 1981.

He has worked with Southwest Research Institute, Allis Chalmers, and Bently Nevada Corporation. He is currently a Full Professor with the Mechanical Engineering Department, Texas A&M University, College Station, TX, USA. His areas of expertise include magnetic bearings, energy storage flywheels, rotordynamics, vibrations, and fuel injector mechatronics.

Dr. Palazzolo is a Fellow of the American Society of Mechanical Engineers (ASME).